ENGINEERING MECHANICS 2004
NATIONAL CONFERENCE
with international participation
Svratka, Czech Republic, 10 - 13 May 2004

NUMERICAL MODELING OF TURBULENT FLOW THROUGH A TURBINE CASCADE

K. Kozel [1] **P. Louda** [2] **J. Příhoda** [3]

Summary: *A model of turbulent flow in subsonic and transonic regime of a turbine cascade using two-equation SST turbulence model is described. The suitable numerical method of its solution, based on implicit AUSM discretization, is given and numerical results for SE 1050 cascade are presented. The influence of turbulence modeling is discussed.*

1. Introduction

We consider a mathematical model of 2D turbulent flow through the SE 1050 turbine cascade. The implicit AUSM finite volume method with SST turbulence model is described and results are presented. The influence of turbulent production is investigated as well.

2. Mathematical model

The model shall solve statistically steady 2D turbulent flow of ideal gas. It is based on averaged Navier-Stokes equations containing mass, momentum, and energy balance. These are obtained using Reynolds averaging for density and Favre (density-weighted) averaging for velocity and internal energy [8]. The system of averaged NS equations is then

$$\int_V \frac{\partial}{\partial t}\begin{bmatrix}\rho\\ \rho u_1\\ \rho u_2\\ \rho E\end{bmatrix} d\mathcal{V} + \oint_{\partial V}(u_c\begin{bmatrix}\rho\\ \rho u_1\\ \rho u_2\\ \rho H\end{bmatrix} + \begin{bmatrix}0\\ pn_1\\ pn_2\\ 0\end{bmatrix})d\mathcal{S} = \oint_{\partial V}\begin{bmatrix}0\\ t_{i1}+\tau_{i1}\\ t_{i2}+\tau_{i2}\\ (t_{ij}+\tau_{ij})u_j - q_i - q_i^t + d_i^t\end{bmatrix} n_i dS$$

$$E = \frac{1}{\gamma-1}\frac{p}{\rho} + \frac{1}{2}(u^2+v^2) + k, \quad H = E + \frac{p}{\rho}, \quad u_c = u_i n_i$$

$$t_{ij} = \mu 2 S_{ij}, \quad S_{ij} = \frac{1}{2}\left(\frac{\partial u_i}{\partial x_j} + \frac{\partial u_j}{\partial x_i}\right) - \frac{2}{3}\delta_{ij}\frac{\partial u_k}{\partial x_k}, \quad q_i = -\frac{\gamma}{\gamma-1}\frac{\mu}{Pr}\frac{\partial(p/\rho)}{\partial x_i}, \tag{1}$$

where V is control volume, n_i outer unit normal vector of its surface, δ_{ij} Kronecker delta, t time, ρ density, u_i velocity vector, E total energy (internal + kinetic of mean flow + kinetic energy of fluctuations), H is total enthalpy, p static pressure, for which equation of state for perfect gas

[1]Prof. RNDr. Karel Kozel, DrSc., Dept. of Technical Mathematics CTU Prague, Karlovo nám. 13, CZ-121 35 Prague 2
[2]Ing. Petr Louda, PhD, Institute of Thermomechanics AS CR, Dolejškova 5, CZ-182 00 Prague 8
[3]Prof. Ing. Jaromír Příhoda, CSc., Institute of Thermomechanics AS CR, Dolejškova 5, CZ-182 00 Prague 8

was used, t_{ij} is stress tensor, and q_i is heat flux vector. The laminar dynamic viscosity, ratio of specific heats, and laminar and Prandtl number are

$$\mu = const, \quad \gamma = 1.4, \quad Pr = 0.72. \tag{2}$$

The turbulent fluctuations are present by Favre averaged Reynolds stress tensor τ_{ij}, turbulent kinetic energy k, turbulent heat flux q_i^t, and turbulent heat transport d_i^t:

$$\begin{aligned} \tau_{ij} &= -\overline{(\rho+\rho')u_i''u_j''}, \quad k = \frac{1}{2\rho}\tau_{ii}, \\ q_i^t &= \overline{(\rho+\rho')u_i''(c_pT)''}, \quad d_i^t = \overline{t_{ij}u_j''} - \overline{(\rho+\rho')u_i''u_j''u_j''/2}, \end{aligned} \tag{3}$$

where quote denotes fluctuation with respect to Reynolds average and double quote fluctuation with respect to Favre average, and overline denotes Reynolds average. These four term need a model expressed by averaged quantities only.

As the sink of mean kinetic energy is the most important influence of turbulence, the Boussinesq' hypothesis for Reynolds stress is used

$$\tau_{ij} = \mu_T 2S_{ij} - \frac{2}{3}\delta_{ij}\rho k, \tag{4}$$

where μ_T is dynamical eddy viscosity. The turbulent heat flux is supposed to have same direction as averaged one, with magnitude rescaled by turbulent heat conductivity related to eddy viscosity through the turbulent Prandtl number Pr_T

$$q_i^t = q_i \frac{Pr}{\mu}\frac{\mu_T}{Pr_T}, \quad Pr_T = 0.91. \tag{5}$$

The additional turbulent transport d_i^t sometimes expressed as diffusion of k (see Eq. (6) below) is neglected in the present study. The model for eddy viscosity is the two-equation SST model of Menter [6]:

$$\begin{aligned} &\int_V \frac{\partial}{\partial t}\begin{bmatrix}\rho k\\ \rho\omega\end{bmatrix} d\mathcal{V} + \oint_{\partial V} u_c \begin{bmatrix}\rho k\\ \rho\omega\end{bmatrix} d\mathcal{S} = \oint_{\partial V}\begin{bmatrix}(\mu+\sigma_k\mu_T)\frac{\partial k}{\partial x_i}\\ (\mu+\sigma_\omega\mu_T)\frac{\partial \omega}{\partial x_i}\end{bmatrix} n_i dS + \\ &\qquad + \int_V \begin{bmatrix} P_k - \beta^*\rho\omega k \\ \frac{\zeta\rho}{\mu_T}P_k - \beta\rho\omega^2 + (1-F_1)\rho\sigma_{\omega 2}\frac{2}{\omega}\frac{\partial k}{\partial x_j}\frac{\partial \omega}{\partial x_j}\end{bmatrix} d\mathcal{V}, \\ &\mu_T = \rho\frac{a_1 k}{\max(a_1\omega, \Omega F_2)}, \quad a_1 = 0.31, \quad \Omega = \sqrt{2\tilde{\Omega}_{ij}\tilde{\Omega}_{ij}}, \quad \tilde{\Omega}_{ij} = \frac{1}{2}\left(\frac{\partial u_i}{\partial x_j} - \frac{\partial u_j}{\partial x_i}\right), \\ &F_1 = \tanh(arg_1^4), \quad arg_1 = \min\left[\max\left(\frac{\sqrt{k}}{0.09\omega y_w}, \frac{500\nu}{\omega y_w^2}\right), \frac{4\sigma_{\omega 2}k}{Cy_w^2}\right], \\ &F_2 = \tanh(arg_2^2), \quad arg_2 = \max\left(\frac{2\sqrt{k}}{0.09\omega y_w}, \frac{500\nu}{\omega y_w^2}\right), \; C = \max\left(\sigma_{\omega 2}\frac{2}{\omega}\frac{\partial k}{\partial x_j}\frac{\partial \omega}{\partial x_j}, 10^{-20}\right) \end{aligned} \tag{6}$$

where ω is specific dissipation rate and the constants are linear combinations $\phi \equiv (\beta^*, \beta, \zeta, \sigma_k, \sigma_\omega) = F_1\phi_1 + (1-F_1)\phi_2$, $\phi_1 = (0.09, 0.0750, 0.5532, 0.85, 0.500)$, $\phi_2 = (0.09, 0.0828, 0.4404,$

$1.00, 0.856)$, and y_w is the distance to the closest wall. The production is

$$P_k = \tau_{ij}\frac{\partial u_i}{\partial x_j} = \mu_T SS - \frac{2}{3}\mu_T\left(\frac{\partial u_k}{\partial x_k}\right)^2 - \frac{2}{3}\rho k\left(\frac{\partial u_k}{\partial x_k}\right),$$
$$S = \sqrt{2\tilde{S}_{ij}\tilde{S}_{ij}}, \quad \tilde{S}_{ij} = \frac{1}{2}\left(\frac{\partial u_i}{\partial x_j} + \frac{\partial u_j}{\partial x_i}\right). \tag{7}$$

The first term $\mu_T SS$ depends on strain rate only, whereas the other two are an effect of compressibility. It is known that the production is overestimated in case of large normal strains (e.g. in front of leading edge of the blade, or in the shock wave). Therefore an ad hoc modification due to Kato, Launder, is also considered:

$$P_k^{KL} = \mu_T S\Omega - \frac{2}{3}\mu_T\left(\frac{\partial u_k}{\partial x_k}\right)^2 - \frac{2}{3}\rho k\left(\frac{\partial u_k}{\partial x_k}\right), \tag{8}$$

where Ω is magnitude of vorticity from (6). In a shear layer, both productions are equivalent, however the modified one is considerably smaller in the problematic regions mentioned. The effect of compressibility remains the same.

The inlet flow is subsonic. The boundary conditions have basically same formulation as for laminar flow in [2]:

- Inlet: given inlet flow angle α_1, stagnation pressure p_0 and density ρ_0, inlet local turbulence intensity Tu and inlet eddy viscosity μ_{T1}, we set

$$u_1/u_2 = \tan(\alpha_1), \quad p\left(1 + \frac{\gamma-1}{2}M^2\right)^{\frac{\gamma}{\gamma-1}} = p_0, \quad \rho\left(1 + \frac{\gamma-1}{2}M^2\right)^{\frac{1}{\gamma-1}} = \rho_0,$$
$$\partial T/\partial n = 0, \quad k = \frac{3}{2}Tu^2(u_1^2 + u_2^2), \quad \omega = \rho k/\mu_{T1}, \tag{9}$$

  where M is local Mach number, T temperature. The value μ_{T1} has been taken $10\mu_T$.

- Wall: The blade surface is adiabatic and smooth. Then

$$u_1 = u_2 = \frac{\partial T}{\partial n} = k = 0, \quad \omega = 9\mu/(\rho\beta_1 y_{w1}^2), \tag{10}$$

  where y_{w1} is a measure comparable with viscous sublayer thickness.

- Outlet: The outlet integral pressure (non-reflecting condition) p_2 is prescribed according to the given outlet isentropic Mach number M_{2is}:

$$\frac{\int_{\partial V_{out}} p d\mathcal{S}}{\int_{\partial V_{out}} d\mathcal{S}} = p_2, \quad \frac{\partial T}{\partial n} = \frac{\partial k}{\partial n} = \frac{\partial \omega}{\partial n} = 0. \tag{11}$$

3. Numerical solution

The system of equations (1), (6) can be rewritten in the form

$$\frac{\partial}{\partial t}\int W d\mathcal{V} + \oint (F^I - F^V) d\mathcal{S} - \int Q d\mathcal{V} = 0, \tag{12}$$

where $F^I,\ F^V,\ Q$ is inviscid flux, viscous flux and source term respectively. For spatial discretization we use a cell centered finite volume method with quadrilateral finite volumes (cells) denoted by indices i, j and composing a structured grid. The unknown W is considered as mean value in the finite volume. The integrals in Eq. (12) are approximated using mid-point rule, leading to

$$\frac{dW_{i,j}}{dt}\Delta V_{i,j} + R(W)_{i,j}\Delta V_{i,j} = 0, \quad R(W)_{i,j} = \frac{1}{\Delta V_{i,j}}\sum_{\alpha=1}^{4}(F^I - F^V)_{i,j,\alpha}\Delta S_{i,j,\alpha} - Q_{i,j}, \tag{13}$$

where $\Delta V_{i,j}$ is area of the cell, $\Delta S_{i,j,\alpha}$ length of its face.

The inviscid flux cell face value is defined using AUSM (Advection Upstream Splitting Method) U-splitting [4].

$$\begin{aligned}
F^I_{1/2} &= u_{c1/2}\begin{bmatrix}\rho\\ \rho u_1\\ \rho u_2\\ \rho H\\ \rho k\\ \rho\omega\end{bmatrix}_{L/R} + p_{1/2}\begin{bmatrix}0\\ n_1\\ n_2\\ 0\\ 0\\ 0\end{bmatrix}, \quad [\cdot]_{L/R} = \begin{cases}[\cdot]_L \text{ for } u_{c1/2} \geq 0,\\ [\cdot]_R \text{ otherwise},\end{cases}\\
u_{c1/2} &= u^+_L + u^-_R, \qquad u^\pm = \begin{cases}\pm\frac{1}{4a}(u_c \pm a)^2 \text{ for } |u_c| \leq a\\ \frac{1}{2}(u_c \pm |u_c|) \quad \text{otherwise}\end{cases}\\
p_{1/2} &= p^+_L + p^-_R, \qquad p^\pm = pu^\pm \cdot \begin{cases}\frac{1}{a}(\pm 2 - \frac{u_c}{a}) \text{ for } |u_c| \leq a\\ \frac{1}{u_c} \qquad\qquad \text{otherwise}\end{cases}
\end{aligned} \tag{14}$$

where $a = \sqrt{\gamma(p + 2\rho k/3)/\rho}$ is effective speed of sound and the normal velocity. The effective pressure $p + 2\rho k/3$ was denoted p for the sake of readability. The advection sensor has been originally proposed as Mach number (M-splitting) [3]. Further, splitting based on mass flux or velocity (U-splitting) has also been published. The present velocity splitting is slightly more diffusive than the M-splitting. In supersonic case, the splitting reduces to full upwinding, whereas in subsonic region, the interface velocity and pressure are basically the same as resulting in van Leer flux vector splitting.

The $L,\ R$ denotes respectively states on the left or right from the interface considered. Taking states in the finite volumes adjacent to the interface, first order upwind is obtained. For higher accuracy needed for turbulent flow computations, the linear extrapolation for conservative variables with limiter was applied. Considering e.g. the face $i + 1/2$ between cells (i, j) and $(i + 1, j)$ we have

$$\begin{aligned}
W_L &= W_{i,j} + \frac{1}{2}\Psi(r_L)\Delta^-, \quad W_R = W_{i+1,j} - \frac{1}{2}\Psi(r_R)\Delta^+,\\
\Psi(r) &= \frac{r + |r|}{r + 1}, \quad r_L = \frac{\Delta + \epsilon}{\Delta^- + \epsilon}, \quad r_R = \frac{\Delta + \epsilon}{\Delta^+ + \epsilon}, \quad \epsilon = 10^{-17},\\
\Delta^- &= W_i - W_{i-1}, \quad \Delta = W_{i+1} - W_i, \quad \Delta^+ = W_{i+2} - W_{i+1},
\end{aligned} \tag{15}$$

where Ψ is the van Leer limiter, switching to first order upwind at occurrence of a local extremum of W (adjacent slopes Δ have opposite sign).

The discretization of diffusive flux is central. The approximation of cell face derivatives needed in diffusive terms uses quadrilateral dual finite volumes constructed over each face of primary volume – the vertices are located at end of primary face and in centres of adjacent primary volumes. The mid-point rule quadrature formula is again used, with face value of velocity defined as average of values in vertices of dual cell [5].

The time discretization uses backward Euler scheme (implicit). First, there is no benefit in solving the two turbulence model equations coupled with Navier-Stokes. The computationally favorable approach of keeping the eddy viscosity, k from previous time level in N-S equations, solving them, and using new velocity in turbulence model equations, has been adopted instead.

Since inviscid as well as viscous and source term are non-linear functions of W, a linearization is needed to obtain linear algebraic system. The Newton linearization with analytically computed Jacobi matrices is used, however only four finite volumes surrounding volume (i,j) are included in the implicit part:

$$\frac{W_{i,j}^{n+1} - W_{i,j}^{n}}{\Delta t} = -R(W^n)_{i,j} - \sum_{\alpha \in S} \frac{\partial R(W^n)_{i,j}}{\partial W_\alpha} (W_\alpha^{n+1} - W_\alpha^n),$$
$$S = \{\, (i,j),\ (i-1,j),\ (i+1,j),\ (i,j-1),\ (i,j+1) \,\} \tag{16}$$

For the linearization of source term in turbulence model a diagonal Jacobi matrix taking into account negative terms in implicit part, has been chosen.

The discretization described above gives a block five diagonal linear algebraic system. It is solved iteratively by a relaxation method with direct block tri diagonal system inversion on selected family of grid lines.

4. Numerical results

Here we consider two regimes of flow through the SE 1050 turbine cascade [7], see Tab. 1. The inlet turbulence intensity is estimated. The finite volume grid is of H-type, containing approx. $34\,000$ finite volumes and refined near the blade (giving aspect ratio up to approx. 800). Details of the grid around leading and trailing edge are shown in Fig. 1. The same grid is used for both regimes.

The Mach number distribution by SST model for both regimes is shown in Figs. 2, 4. The difference in Mach number for modified turbulence production is negligible. The results compare well with measurements as well as laminar results of several different schemes [1].

The distributions of pressure and friction on the blade surface are shown in Figs. 3, 5, where the results by turbulence model with modified production (8) are denoted mod. SST. The difference between the two models is marginal here, except for friction around leading edge. The influence of turbulence production term is best seen on turbulence energy distribution in the presence of shock wave, Fig. 6. The improvement around leading edge in mod. SST has been already mentioned. On the other hand the normal strains cause an increase of k in the shock wave as well (left sub-figure) and if the production is P_k^{KL} but with neglected influence of compressibility, then just almost nothing happens in the shock wave (middle sub-figure). However the compressibility further diminishes the production, therefore using P_k^{KL} from (8) leads to

Tab. 1: Flow regimes

	M_{2is}	p_2/p_0	α_1	Re_2 (chord l.)	wall	Tu
subsonic:	0.716	0.7106	$19.3°$	$1.50 \cdot 10^6$	adiabatic	$2\,\%$
transonic:	1.198	0.413	$19.3°$	$1.24 \cdot 10^6$	adiabatic	$2\,\%$

Tab. 2: Energy loss coefficient

	measured	SST	mod. SST
subsonic:	$3.75\,\%$	$2.85\,\%$	$2.81\,\%$
transonic:	$4.70\,\%$	$2.67\,\%$	$2.70\,\%$

decrease of k past the shock wave. This result seems unphysical. Although P_k^{KL} might improve the blade surface parameters, the turbulence intensity inside the flow-field can even be qualitatively wrong.

The energy loss coefficient ξ is evaluated according to

$$\xi = 100(1 - \lambda_2^2/\lambda_{iso2}^2),$$
$$\lambda_2^2 = \frac{\gamma+1}{2}\left[1 + \frac{\gamma-1}{2}M_2^2\right]^{-1} M_2^2, \quad \lambda_{iso2}^2 = \frac{\gamma+1}{\gamma-1}\left[1 - \left(\frac{p_2}{p_0}\right)^{\frac{\gamma-1}{\gamma}}\right], \tag{17}$$

where $M_2,\ p_2$ are mean values at line located 1/3 of the pitch downstream of trailing edge. The results and comparison with measurement is given in Tab. 2. Although it should be remarked this parameter is extremely sensitive to details of evaluation, poor agreement (even opposite Mach number dependence) with measurements is apparent. The cause is not known at time.

Acknowledgment

This work was supported by the project K276106 and by the project CFD-QNET network sponsored by the European Community under contract No. G1RT-CT-2000-05003, and grant 201/01/0684 of GA CR.

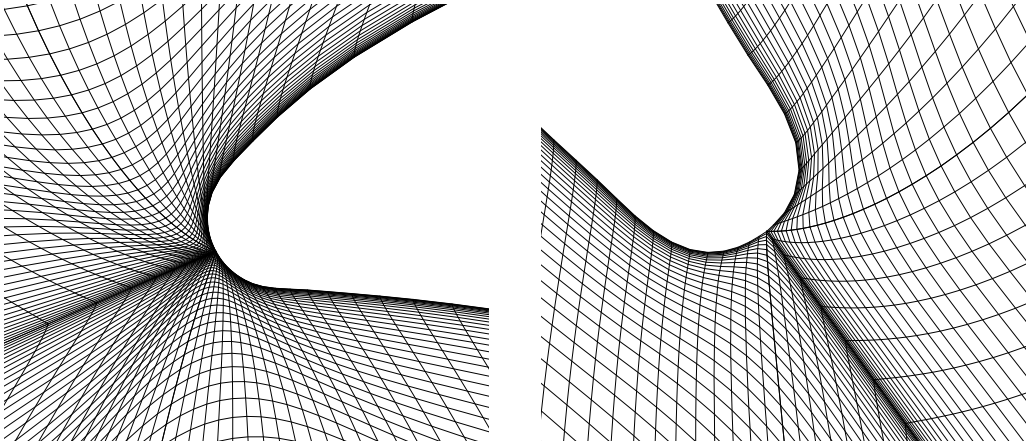

Fig. 1: Detail of grid around leading (left) and trailing edge (right)

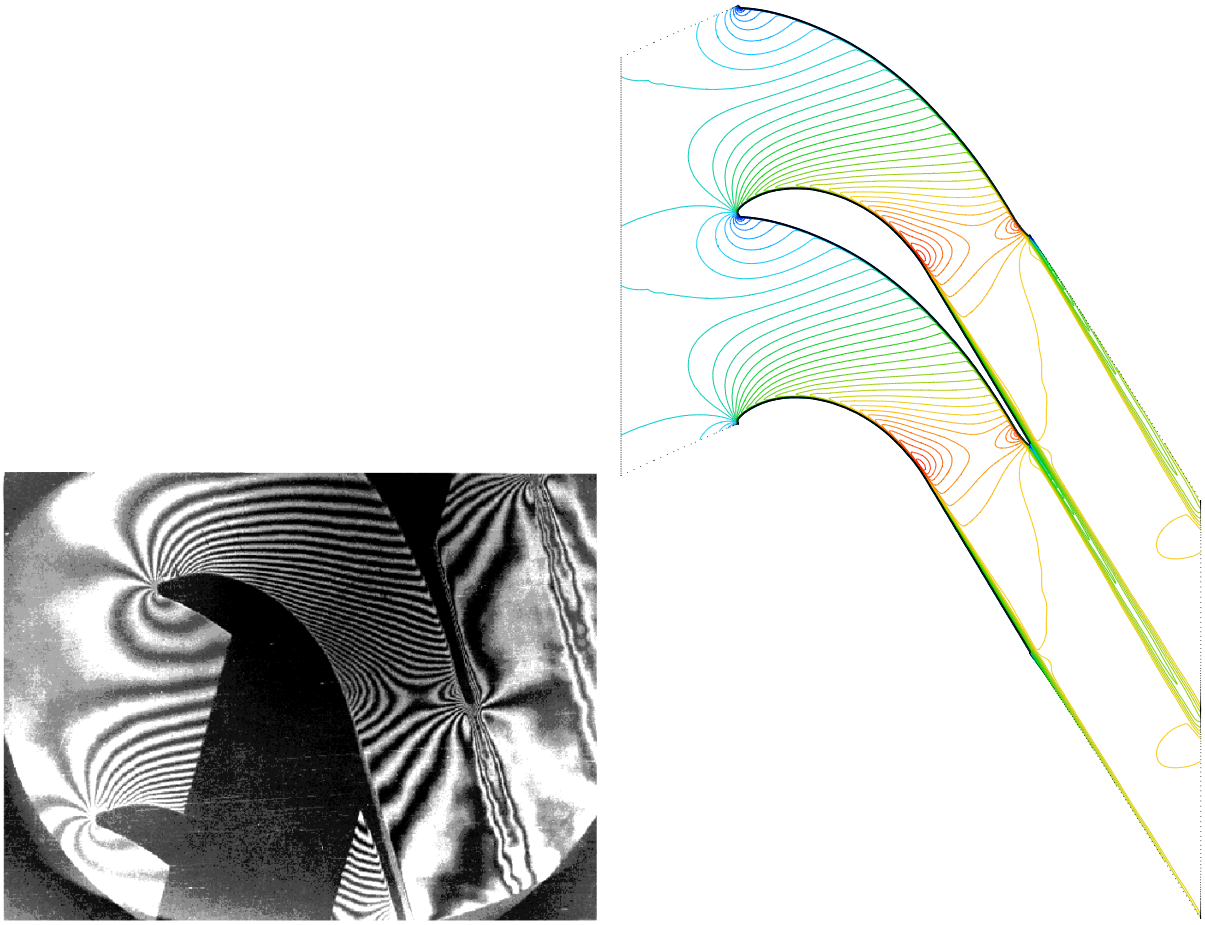

Fig. 2: Subsonic case: interferometric view [7] (left) and isolines of computed Mach number (right)

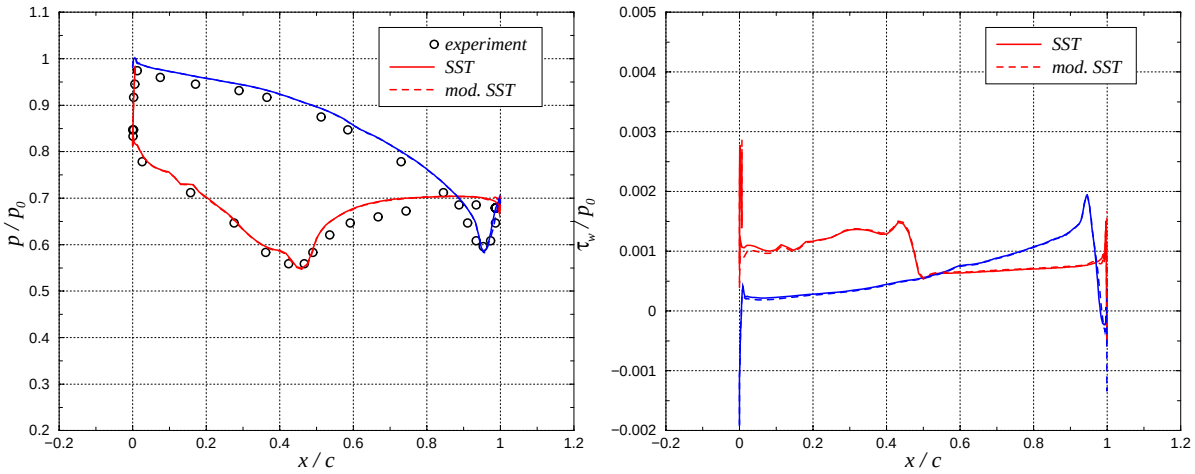

Fig. 3: Pressure and friction on the blade surface, subsonic case

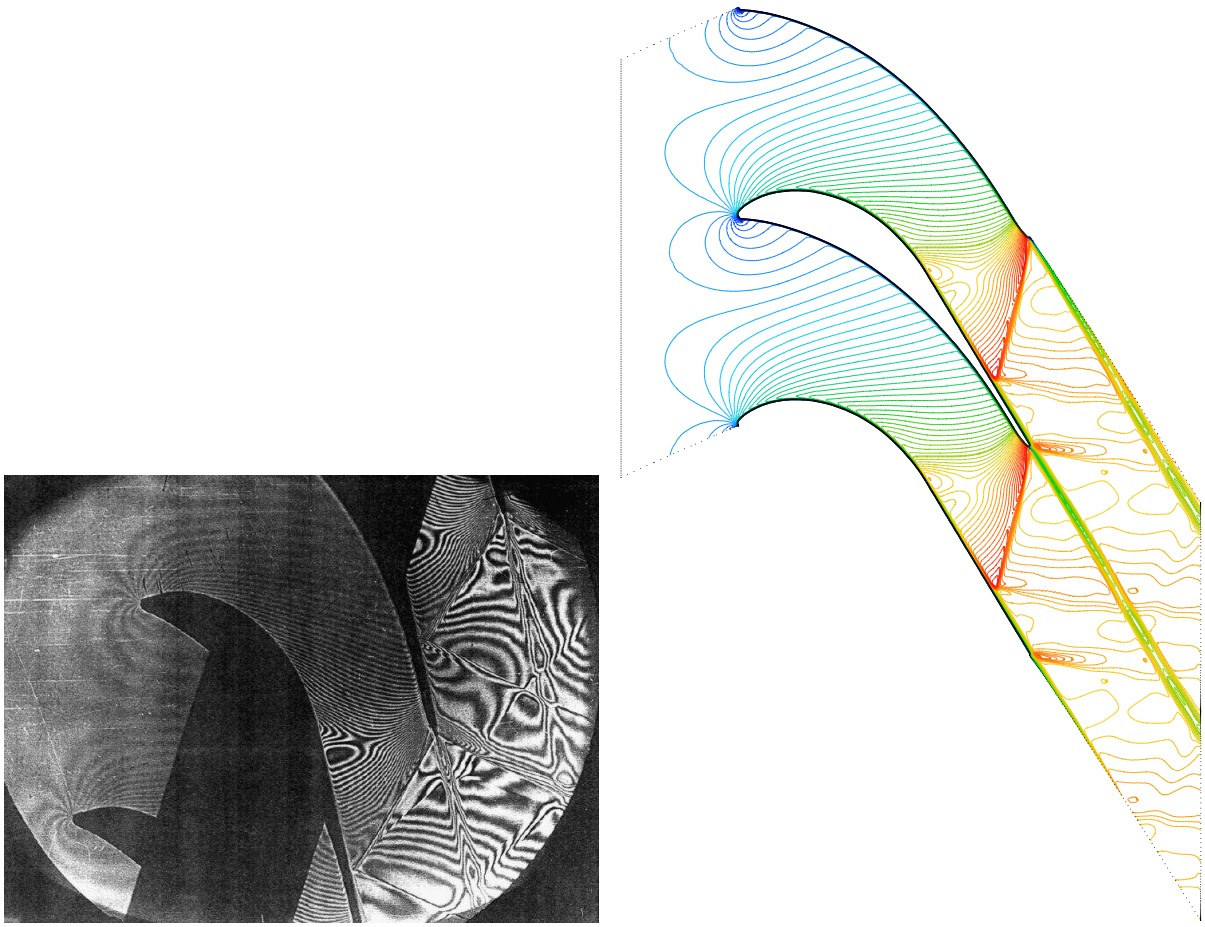

Fig. 4: Transonic case: interferometric view [7] (left) and isolines of computed Mach number (right)

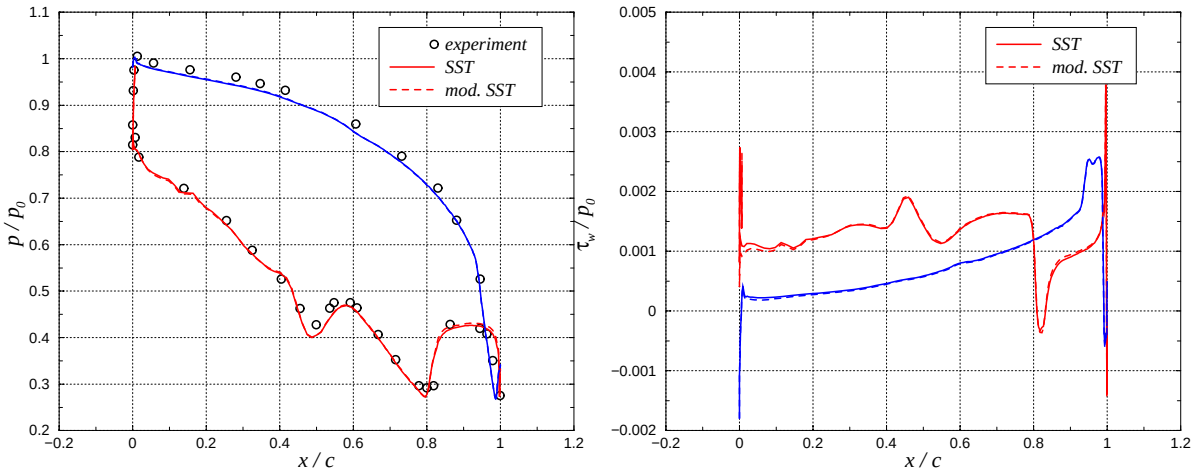

Fig. 5: Pressure and friction on the blade surface, transonic case

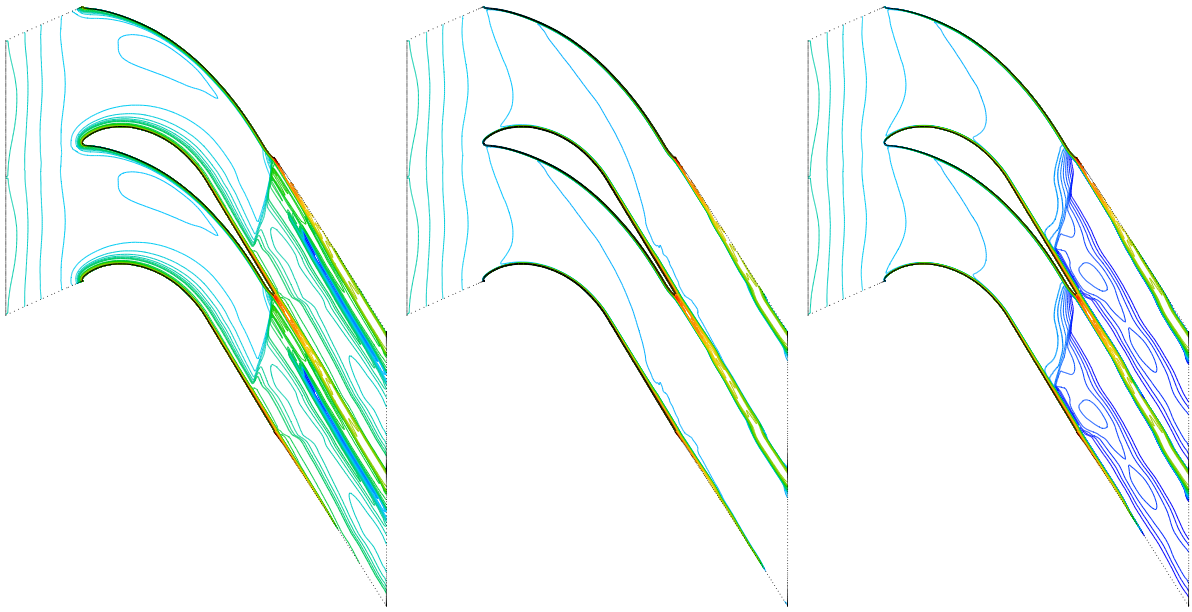

Fig. 6: Turbulent kinetic energy for transonic case and different production of turbulence: standard (left), Kato-Launder with no compressibility effect (middle), and Kato-Launder (right)

References

[1] Dobeš J., Fořt J., Fürst J., Halama J., Kozel K. (2003) Numerical solution of transonic flows in 2D and 3D axial and radial turbine cascades. in: 5th European conference on turbomachinery, Prague, pp. 1105–1114.

[2] Fürst J. (2000) Numerical solution of transonic flows using TVD and ENO schemes. PhD thesis, University of Aix-Marseille II and FME CTU Prague.

[3] Liou M.-S., Steffen C. J. (1993) A new flux splitting scheme. J. Comp. Phys.., 107:23–39.

[4] Liou M.-S. (1993) On a new class of flux splittings. Lecture Notes in Phys., 414:115–119.

[5] Louda P. (2002) Numerical solution of 2D and 3D turbulent impinging jet flow, PhD thesis, FME CTU Prague, (in Czech).

[6] Menter, F. R. (1994) Two-equation eddy-viscosity turbulence models for engineering applications. AIAA J., 32(8):1598–1605.

[7] Šťastný M., Šafařík P. (1990) Experimental analysis data on the transonic flow past a plane turbine cascade. ASME Paper No.90-GT-313, New York.

[8] Wilcox, D. C. (1994) Turbulence modeling for CFD. DCW Industries, Inc., California.